https://doi.org/10.2352/ISSN.2169-2629.2018.26.134

A Robust Algorithm for Computing Boundary Points of the Metamer Mismatch Body

Tarek Stiebel, Dorit Merhof
Institute of Imaging & Computer Vision, RWTH Aachen University, Germany

Abstract

Metamer mismatching is a challenging element of both human and machine color vision. In this work, the theory yielding the description of the metamer mismatch body proposed by Logvinenko [1] is revisited. An algorithm is proposed capable of robustly solving the original equations which precisely describe the boundary of the metamer mismatch body. Additionally and in contrast to before, the requirement for illuminants to be strictly positive is suspended. This is achieved by no longer associating boundary points of the metamer mismatch body with optimal reflectance functions.

The algorithm has been abstracted to deal with sensors of arbitrary dimensionality, making it applicable to multi-spectral imaging.

Introduction

Metamerism describes the phenomenon that different objects may appear in the same color to a human observer, although their spectral reflectance functions do not actually match. Unfortunately, this proves to be problematic in many applications. For example, while all these different objects appear identical to one observer, they may differ significantly to another observer. This effect is known as *metamer mismatching* [2] and may either be caused by a change of the observer (observer-induced), by a change of the illuminant (illuminant-induced) or by a combination of both. It always occurs if the Luther-Ives condition is broken [3, 4], e.g. in the observer-induced case this is due to to the fact that the relationship between the respective color-matching functions cannot be represented by a linear transformation. Instead of a direct correspondence between tristimulus values of the respective observers, a tristimulus value maps to an entire set of possibilities called the *metamer mismatch volume/body* (MMB) [2, 5]. Thus, enforcing an actual point-to-point transformation most likely introduces a color error. While the concept of metamerism was originally motivated by human vision and is therefore, strictly speaking, restricted to human observers, it can be equivalently applied to a general camera system defined by its spectral sensitivity functions. It is also possible to have a combination of human observers and camera systems. Creating and reproducing high-fidelity color images is a typical example, where pictures of an arbitrarily illuminated scene taken by a camera are reproduced on a monitor. The monitor is viewed by the human observer, who should perceive the color image on the monitor just as in the original scene. The conversion of measured camera signals towards a human observer, usually in the form of CIE XYZ coordinates, is a well known challenge commonly referred to as *color management*, which has been subject to extensive previous research.

All proposed methods can be divided into two classes, namely target-based and model-based [6]. The former tries to determine a relationship based on a set of known correspondences. In the simplest case a linear transformation is chosen using regression techniques to minimize an error metric of choice [7, 8]. Due to the general non-linearity of the actual dependence, such an approach potentially results in large color errors. More sophisticated methods aim at describing the relationship using more general functions such as polynomials [9] or make use of neural networks [10].

Model-based methods on the other side consider the actual physical process of image acquisition. They minimize the introduced color difference by estimating central positions inside the MMB [1, 6, 11].

Although there has been a lot of practical as well as theoretical interest in the calculation of MMBs, it is a difficult task to actually perform this calculation and, therefore, remained an unsolved problem for a long time. Approximate solutions existed, but it is hard to judge how good these approximations actually are due to the lack of reference data. Logvinenko [1] is the first to provide the theory in form of a set of equations precisely describing the MMB in terms of its boundary. The only restrictions are that the illuminant as well as the sensitivity functions need to be strictly positive. However, finding solutions to these set of equations is complicated. It is yet unclear how to find a specific solution in the general case both in a fast and a robust way, making it hard to apply the proposed theory over large datasets. In order to simplify the calculations an approximation was introduced, which has been called the (n-1)-transition approximation [1]. It has been argued, that the (n-1)-approximation is accurate enough.

The key contribution of this paper is twofold. First of all, an extended interpretation of the theory introduced by Logvinenko [1] is given. By rethinking the underlying geometry of the MMB, the originally essential restriction [1] that the spectral power distribution of the light source needs to be strictly positive is suspended. This is achieved by no longer describing the boundary of the MMB in terms of its surface, but instead through inequality constraints.

Second, a novel algorithm is proposed which allows the precise computation of boundary points of the MMB for any pair of spectral sensitivity functions and illuminants. This algorithm can be used to robustly find solutions of the original theory in the general case within fractions of a second. The proposed algorithm has been generalized to camera systems of arbitrary dimensionality.

Known Theory

Human observers and cameras will not be distinguished since there is no difference from a mathematical point of view. Instead, both of them will be referred to using the generic term of a *sensing device*. A widely used model describing the creation process of a *color signal*, $\Phi = (\varphi_1, ..., \varphi_q)$, for a q-dimensional sensing device is

$$\varphi_i(r) = \int_{\lambda=\lambda_{min}}^{\lambda_{max}} \sigma_i(\lambda) r(\lambda) d\lambda \quad (i = 1, ..., q), \tag{1}$$

where r denotes the spectral reflectance of the viewed object and $\sigma_i(\lambda) = s_i(\lambda) l(\lambda)$ is known as the *spectral weighting function* in the US industry. s_i denotes the spectral sensitivity function of the i'th color channel and l denotes the spectral power distribution of the light source.

The combination of a sensing device and an illuminant will be called a *color-mechanism* [1]. A color mechanism is always associated with its spectral weighting functions. All spectral weighting functions form a parametric cure $\boldsymbol{\sigma} : \lambda \to \mathbb{R}^q$, $\boldsymbol{\sigma}(\lambda) = (\sigma_1(\lambda), ..., \sigma_q(\lambda))^T$ called the *spectral curve*.

Neglecting fluorescent objects and, strictly speaking, gloss, the wavelength dependent reflectance, $r(\lambda)$, has to be in the range [0, 1] to be physically plausible. Let R denote this set of all physically plausible reflectances. On an abstract level, Equation 1 can be seen as a linear map $\Phi : R \to \mathbb{R}^q$. Of particular interest is the set of all possibly achievable color signals, the so-called *object color-solid* $\Phi(R)$ (OCS) [2].

Metamer Mismatching

Two objects, $r_1(\lambda)$ and $r_2(\lambda)$, are said to be metameric with respect to a color mechanism $\Phi(r)$, if they lead to the same color signal, i.e. $\Phi(r_1) = \Phi(r_2)$. While all these metamer reflectances induce the same color signal in Φ, the same might not be true for another color mechanism, Ψ.

Consider the case of two different color-mechanisms $\Phi = (\varphi_1, ..., \varphi_q)$ and $\Psi = (\psi_1, ..., \psi_w)$ which are assumed to be linearly independent of each other. Let r_0 denote the spectral reflectance function of an object which in turn is viewed by the first mechanism, i.e. $\mathrm{x}_0 = \Phi(r_0)$. The MMB associated with the change of color-mechanisms from Φ to Ψ is given by $M(r_0, \Phi, \Psi) = \Psi(\Phi^{-1}(\Phi(r_0)))$ [1]. Expressed in words, the set of all reflectance spectra metameric to r_0 with respect to Φ is constructed in a first step, i.e. $\Phi^{-1}(\Phi(r_0))$. Subsequently, the set is mapped onto Ψ leading to the MMB.

Constructing the unified color-mechanism $\mathrm{U} = (\Phi; \Psi) = (\varphi_1, ..., \varphi_q, \psi_1, ..., \psi_w)^T = (u_1, ...u_n)^T$ with $n = q + w$ results in the MMB being a cross section of $\mathrm{U}(R)$ [1],

$$M(r_0, \Phi, \Psi) = \{\mathrm{z} \in \mathbb{R}^w : (\mathrm{x}_0; \mathrm{z}) \in \mathrm{U}(R)\}. \tag{2}$$

The boundary of the MMB is given by all points located on the boundary of the OCS with respect the unified observer, U, mapping onto x_0 in the Φ-subspace of U [1].

Assuming the illuminant is strictly positive, boundary points of the OCS can be uniquely associated with spectral reflectances. If a boundary point of the OCS can be uniquely associated with a reflectance function, the reflectance is called an *optimal reflectance*. The boundary point is in the context of human vision known as an *optimal color*. It has been known for a long time that optimal reflectance functions can only take the values 0 or 1 [12] and are of the form of elementary step functions. Whenever the function value of an optimal reflectance function changes from zero to one (or vice versa) a so-called transition happens. The corresponding wavelengths are known as *transition wavelengths*. In the general case, there might be an arbitrary amount of them. An optimal reflectance function with respect to the color mechanism U will be denoted by $r_U(\lambda_t)$, where λ_t denotes the transition wavelengths.

With the help of optimal reflectance functions, the boundary of the MMB can be described as

$$\Phi(r_U(\lambda_t)) = \mathrm{x}_0. \tag{3}$$

It is shown in [1] how to expand this equation to describe a precise boundary point of the MMB in a chosen direction from a point inside the MMB.

Equation 3 has the limitation that it describes the boundary of the MMB in terms of optimal reflectance functions. Therefore, it is essential that each boundary point of the OCS of the unified color mechanism can in fact be uniquely associated with an optimal reflectance function. This is only the case, if illuminants are not allowed to become zero. Otherwise, the notion of optimal reflectance functions ceases to exist. Boundary points of the OCS can no longer be uniquely associated with spectral object reflectances in the general case, but instead there possibly exists an infinite set of reflectances mapping onto the same boundary point. Boundary points become metameric themselves, leading to the essential constraint of illuminants needing to be strictly positive.

The (n-1)-transition approximation

Although Equation 3 describes a precise boundary point of the MMB, it is not trivial to actually solve the equation in the general case. Optimization techniques may be employed. However, such optimizations are slow and, most importantly, there is no guaranteed convergence. In order to simplify the process of calculation, another approximation to the OCS boundary was introduced, namely the (n-1)-approximation [1]. Assuming the n-dimensional color mechanism U, only the set of all elementary step functions having equal or less than n transition wavelengths is considered. This set is denoted by O_n. The resulting volume $\mathrm{U}(O_n)$ is then called the (n-1)-transition approximation to the OCS. Based on the (n-1)-transition approximation, an algorithm was proposed, allowing to calculate boundary points of the MMB in chosen directions [1].

New Algorithmic Approach

In this section, a different way of describing the boundary of the MMB in chosen directions will be proposed which does not rely on the existence of any optimal reflectance function. The originally essential constraint for the illuminant to be strictly positive is overcome. The resulting algorithm is able to robustly locate a boundary point of the MMB in any chosen direction independent of the illuminant or sensitivity function in a very short time. All of this achieved without introducing any simplification like the (n-1)-transition approximation.

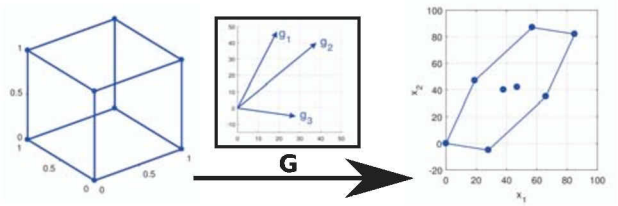

Figure 1: In the visualized exampled, a 2D Zonotope is constructed by the projection of a 3D Cube.

Dual Object Color-Solid

It is known that the set of all spectral object reflectances being within the range [0, 1] forms a hypercube. Given a color mechanism, the construction of the OCS can be interpreted as the projection of this hypercube onto the subspace the OCS of the color mechanism is located in. The projection is defined by the spectral weights associated with the color mechanism.

An exemplary projection of a 3D-cube onto 2D space is shown in Figure 1. The entity created this way is known as a Zonotope and described by

$$Z = \{\mathbf{G}\mathrm{c} \mid c_i \in [0,1] \forall i\}, \tag{4}$$

where $\mathbf{G} = [g_1, ..., g_d]$ and $\mathrm{c} = (c_1, ..., c_d)^T$. The column vectors making up the projection matrix $\mathbf{G}$ are known as generators. A Zonotope is always point symmetric.

However, an d-dimensional hypercube can also be interpreted as a set of inequality constraints

$$C = \{\mathrm{c} \in \mathbb{R}^d \mid 0 \leq c_i \leq 1 \; \forall \, i = 1, ..., d\}, \tag{5}$$

where each individual constraint represents a hyperplane tangent to the hypercube. Our approach is based on exactly these inequality constraints, yielding the hypercube, but transferred into the subspace the zonotope is located in given the projection defined by the spectral weights. However, this transferring of inequality constraints, is not as straightforward as a simple projection of the corner points of the hypercube. In fact, it is an impossible task to achieve directly. What is possible though, is (in analogy to describing boundary points of the OCS in a chosen viewing direction) to compute hyperplanes having a chosen normal vector such that they are tangent to the zonotope. In fact, both approaches are heavily related to each other.

Let the dimensionality of a considered color mechanism be n. Given an arbitrary n-dimensional hyperplane, it can be reprojected into the d-dimensional space of the hypercube. By choosing an arbitrary normal vector $\mathrm{k} \in \mathbb{R}^n$, there is one degree of freedom left for a possible hyperplane, namely the distance to the origin. This degree of freedom can be fixed by the fact that the reprojection of the hyperplane into $\mathbb{R}^d$ must be tangent to hypercube. There will always exist two of such hyperplanes and they can be computed using (adopting notation from projective geometry [13])[1]

$$\begin{aligned} \tilde{\mathrm{H}}_1(\mathrm{k}) &= \mathbf{T}_{cent}^{-T} \begin{pmatrix} \mathrm{k} \\ +\frac{1}{2}\sum_{i=1}^{n} |\mathrm{k}^T \mathrm{g_i}| \end{pmatrix}, \\ \tilde{\mathrm{H}}_2(\mathrm{k}) &= \mathbf{T}_{cent}^{-T} \begin{pmatrix} \mathrm{k} \\ -\frac{1}{2}\sum_{i=1}^{n} |\mathrm{k}^T \mathrm{g_i}| \end{pmatrix}, \end{aligned} \tag{6}$$

[1]Given the point $\tilde{\mathrm{z}} \in \mathbb{P}^n$ and the hyperplane $\tilde{\mathrm{h}} \in \mathbb{P}^n$, the point is located on the plane if $\tilde{\mathrm{h}}^T \tilde{\mathrm{z}} = 0$

with the matrix $\mathbf{T}_{cent}$ representing a simple translation taking the origin to the point of symmetry of the zonotope, ζ_s,

$$\mathbf{T}_{cent} = \begin{bmatrix} 1 & .. & 0 & \zeta_{s1} \\ 0 & \ddots & \vdots & \vdots \\ \vdots & \ddots & 1 & \zeta_{sd} \\ 0 & ... & 0 & 1 \end{bmatrix}. \tag{7}$$

In order to demonstrate the meaning of Equation 6, the Zonotope of Figure 1 is considered again. The three generators as well as an exemplary normal choice are drawn in blue and black in Figure 2a. For visualization purposes only, the length of the normal exceeds zero. For each pair of normal vector and generator, their dot product can be seen as the projection of the generator onto the normal as visualized in Figure 2a. If all positive dot products are added up, the result is the distance of the hyperplane having the normal vector k to the origin, such that it is tangent to the zonotope. Analogously, if all negative dot products are added, the distance of the complementary hyperplane to the origin is obtained. Both of these hyperplanes are drawn in purple in Figure 2b.

Up until now, a very important property of the zonotope has been neglected, namely its point symmetry. The distance of both hyperplanes to each other is obviously the sum of the absolute value of all dot products. Due to the point symmetry of the zonotope, the distance of each hyperplane to the symmetry point of the zonotope is equal and therefore half of the distance in between both hyperplanes. This is exactly what Equation 6 describes, neglecting the transformation matrix. The hyperplane

$$\tilde{\mathrm{H}}(\mathrm{k}) = \begin{pmatrix} \mathrm{k} \\ \frac{1}{2}\sum_{i=1}^{n} |\mathrm{k}^T \mathrm{g_i}| \end{pmatrix} \tag{8}$$

is tangent to the desired zonotope with the important difference that the zonotope would be translated such that it is centered around the origin. The translation matrix does nothing more than translating the hyperplane back to its correct position in space.

Abstraction of the discrete case to the continuous version is possible. Applied to the theory of metamer mismatching and given the color mechanism Φ, a hyperplane pair tangent to the OCS can be computed from a normal choice using

$$\begin{aligned} \tilde{\mathrm{p}}_p(\mathrm{k}_\Phi) &= \mathbf{T}_{cent} \begin{pmatrix} \mathrm{k}_\Phi{}^T \\ -\frac{1}{2}d \end{pmatrix}, \\ \tilde{\mathrm{p}}_n(\mathrm{k}_\Phi) &= \mathbf{T}_{cent} \begin{pmatrix} \mathrm{k}_\Phi{}^T \\ +\frac{1}{2}d \end{pmatrix}, \end{aligned} \tag{9}$$

where

$$d = \int_{\lambda_{min}}^{\lambda_{max}} |\mathrm{k}_\Phi{}^T \sigma(\lambda)| d\lambda \tag{10}$$

represents the distance of both tangent hyperplanes to each other. The very essential gain in mapping the normal vector to a tangent hyperplane pair (Equation 9) instead of to boundary points is that it is completely independent of the possible existence of optimal reflectance functions. Each of those tangent hyperplanes can be seen as an inequality constraint. Even if optimal reflectance functions fade from existence, the inequality constraints remain.

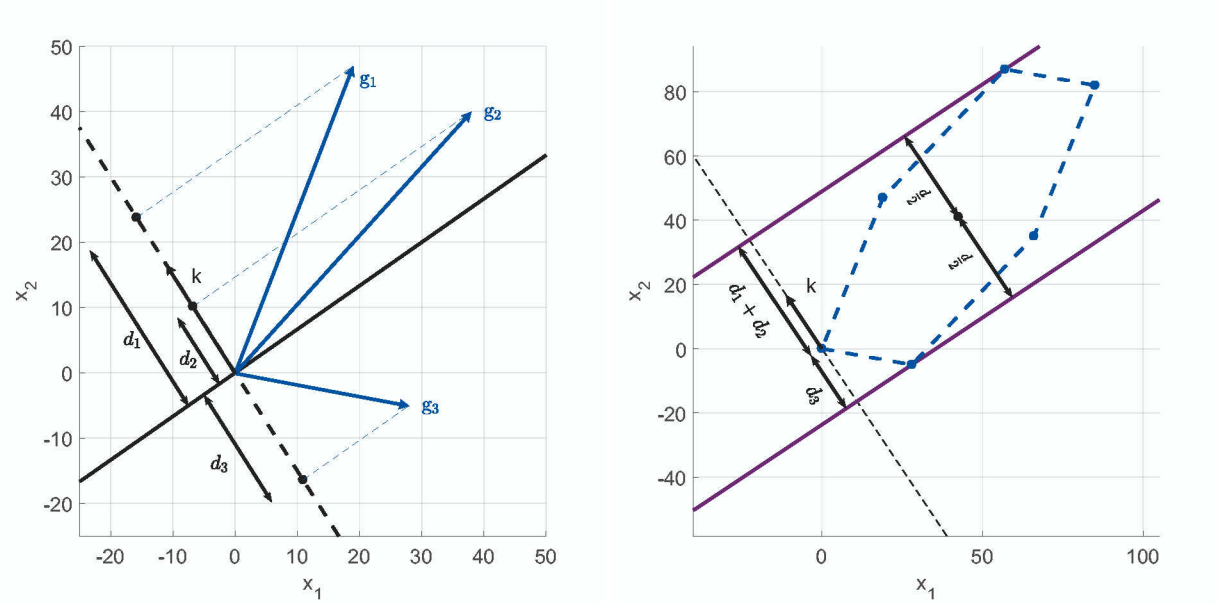

(a) The dot product between generators and a normal choice (b) Zonotope

Figure 2: Visualization of the dual construction.

Calculating the MMB Boundary

Assuming a random point inside the MMB is known, the boundary of the MMB is sought in a specific viewing direction from this point of view. Let a single viewing direction be denoted as the visual ray. An arbitrary normal choice, $\mathrm{k_U}$, can be mapped to a hyperplane tangent to the OCS. This hyperplane intersects the visual ray in exactly one point. Finally, it is only required to minimize the distance of the central point to this intersection. This approach is visualized in Figure 3d. For this purpose, a simple 2D example is considered in form of two one-dimensional color-mechanisms, Φ and Ψ, which are assumed to consist of the CIE standard color matching function $\tilde{y}(\lambda)$ under the illuminants A and D65, respectively. Additionally, values of the illuminant for the second observer were simply set to zero. It is a basic example of illuminant induced metamer mismatching. The corresponding spectral weighting functions are shown in Figure 3a, the spectral curve of the unified observer is shown in Figure 3b and the resulting OCS is shown in Figure 3c.

Assuming the color-signal $\Phi_0 = 20$ is induced in the color-mechanism Φ, Figure 3d displays our approach in calculating boundary points of the resulting MMB. The boundary of the OCS is drawn in blue, the color-signal $\Phi_0 = 20$ is visualized in red and corresponds to the line $\tilde{\mathrm{h}}_1$ in Figure 3d intersecting the boundary of the OCS in exactly two points. Directly optimizing a boundary point such that it is located on $\tilde{\mathrm{h}}_1$, is in case of the lower boundary point not possible at all, since such a point simply cannot be expressed using the original theory.

Instead of a boundary point, the respective tangent hyperplane $\tilde{\mathrm{p}}_\mathrm{p}(\mathrm{n_U})$ is constructed and intersected with $\tilde{\mathrm{h}}_1$. The intersection is marked in black, all tangent hyperplanes are visualized in purple. Given an arbitrary point inside the MMB, U_c, the boundary of the MMB minimizes the distance of U_c to the intersection. The distance as function over the normal choice $\mathrm{k_U}$, which in turn can be parametrized by a single angle α since $|\mathrm{k_U}| = 1$, i.e. $\mathrm{k_U} = (\cos(\alpha), \sin(\alpha))^T$, is plotted in Figure 3e.

However, the major advantage of this approach for locating the MMB boundary is the shape of the error function, as shown in Figure 3e. The function is respectively piecewise convex and concave, making it extremely easy for any optimization technique to robustly find the optimal values. Even more, this function property can be mathematically proven in the general case.

Application

The proposed algorithm has been implemented in Matlab. The optimization was performed using the Nelder-Mead Algorithm. As the very first step, the proposed theory and the resulting algorithm were validated using the original theory [1]. Both the original as well as the proposed algorithm allow to sample the boundary surface in dedicated directions. However, although the original theory describes the precise MMB in form of a set of equations (Eq. 9 and 10 in [1]), it is unclear how to reliably find a solution in the general case. This is what originally motivated the re-parametrization including the introduced (n-1)-approximation. Comparing the results of the proposed algorithm to the results of the original theory is therefore difficult when considering a large data set.

The validation is performed by considering the case of illuminant induced metamer mismatching for a human standard observer when changing the illuminant from A to D65, leading to the two color mechanisms Φ^A and Ψ^{D65}. Since the illuminants are strictly positive, the proposed as well as the original theory should yield identical results. Assuming Φ^A views the gray reflectance $r_g(\lambda) = 0.5$, the MMB $M(r_g, \Phi^A, \Psi^{D65})$ is calculated once using the original theory and once using the proposed algorithm.

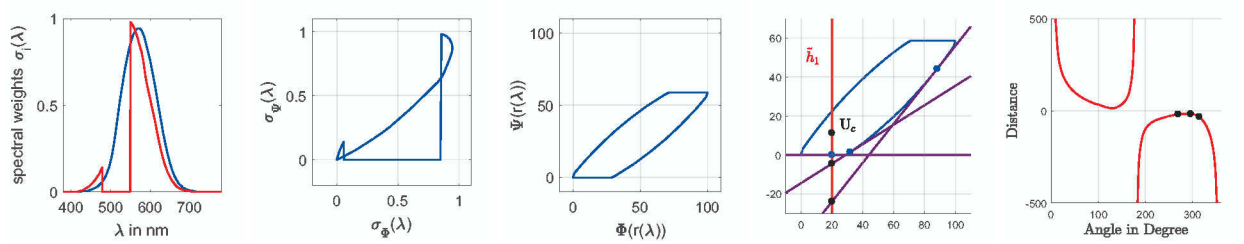

(a) Spectral Weighting Functions (b) Spectral Curve (c) OCS (d) OCS (e) error function

Figure 3: Construction of the metamer mismatch body.

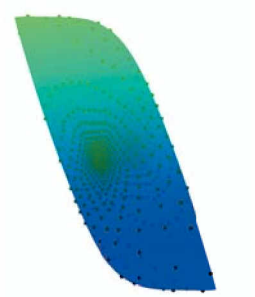

Figure 4: Comparison of the proposed calculation to the ground truth.

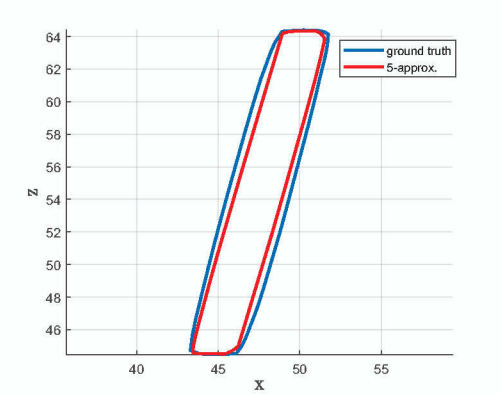

Figure 5: Comparison of the 5-transition approximation to the ground truth.

Using the proposed algorithm, the boundary surface of the MMB was sampled from a central point within and using an icosahedron with a tesselation order of three, which corresponds to 642 points uniformly distributed over a spherical surface. The method employed to generate the ground truth consists of a two step approach. It is significantly simpler to only find points which are located on the boundary of the MMB, independent of where they are located exactly. Based on random, but distinct initial values, a respective optimization was performed using the original theory until a set of 1000 boundary points was found. In addition, an optimization was performed taking the results of our proposed algorithm as initialization. They were then optimized such that they are again located on the MMB but this time as close as possible to the desired sampling points. The combination of both point sets forms our ground truth.

Figure 4 visualizes the resulting MMB by showing all the computed boundary points using the proposed algorithm and the convex hull of all points calculated using the original theory. The Euclidean distance of all boundary points calculated using the proposed algorithm to the convex hull of the point set calculated using the original theory is computed. The average Euclidean distance is 0.0039 with the maximum distance being 0.04. These values can be seen as a perfect match, especially when considering that often, there is a small angular offset between the points of the ground truth and our method.

Accuracy of the $(n-1)$-transition approximation

Next, the influence of the $(n-1)$-transition approximation to the MMB is analyzed. The same case of illuminant induced metamer mismatching as before in combination with the gray spectral reflectance. The 5-transition approximation was generated the same way as in the original paper. A total amount of 1000 points randomly distributed over the boundary surface of the 5-transition approximation to the MMB was calculated for each spectral reflectance.

The results are compared to the ground truth of the previous section in two different ways. First of all, the Euclidean volume of the approximation to the MMB is computed using the convex hull of all boundary points. This volume is set in relation to the volume of the ground truth. The (n-1)-approximation was found to be only 81.66% accurate for the considered example.

Second, the distances of all computed boundary points based on the approximation to the ground truth were computed. A lot of points are located on the inside of the MMB. The average distance of all points to the ground truth is 0.12, the maximum distance is 0.57. This effect is certainly expected, since boundary points of the MMB can only be accurately described by the approximation, if they are associated with optimal reflectance functions having not more than 5-transitions. In general, this is not the case. Figure 5 displays a slice through the three dimensional boundary ($Y = 50$), which was computed using the approximation in comparison to the ground truth. While in some directions (top and bottom) the computed boundaries are located precisely on top of each other, most of the approximated points are on the inside of the MMB.

Partially Zero Illuminants

In contrast to before, the proposed algorithm allows to calculate MMBs even if the illuminant has zero emissions in certain wavelengths. This is demonstrated by considering the same case

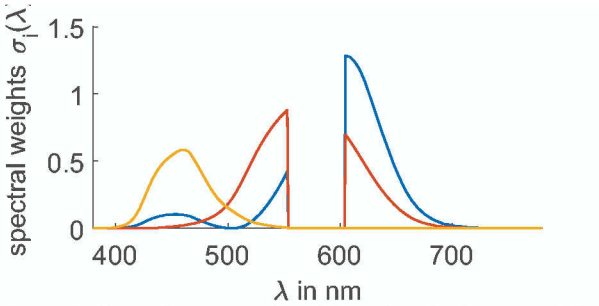

Figure 6: Exemplary spectral weights when having a partially zero illuminant

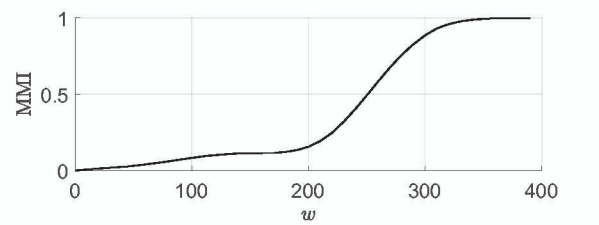

Figure 7: Effect of having a partially zero illuminant

of illuminant induced metamer mismatching as before, but setting the illuminant of the first color mechanism, Φ^A, to zero within a certain wavelength interval. The interval is centered around 580nm and may have different widths, w. An example of the resulting spectral weights in case of a width of $w = 50$nm is shown in Figure 6. The width of the interval was increased from being non existent to cover the entire wavelength range. For each width, the associated MMB was computed when viewing the gray surface $r(\lambda) = 0.5$.

The MMBs were quantified in terms of the metamer mismatch index (MMI) [1], which is defined as the Euclidean volume of the MMB in relation to the Euclidean volume of the OCS. Figure 7 displays the development of the MMI over the width. The MMI does increase the more the wider the interval of zeros becomes. This behavior is most intuitive, since the wider the blind spot becomes, the more uncertainty will be introduced. However, the curve also allows to predict the importance of different wavelength areas in terms of its derivative. For example, increasing the width from 120nm to 180nm does hardly have any effect. The MMI increases more or less strong over the width depending on the importance of the sensitivity in the wavelength areas currently faded out.

Conclusion

An algorithm has been proposed which is capable of calculating the precise boundary of the metamer mismatch body associated with a change of color-mechanisms for arbitrary illuminants as well as sensor sensitivity functions. The originally essential constraint that the illuminant has to be strictly positive is suspended. This was achieved by describing the object color-solid as the projection of a hypercube. Transferring the inequality constraints yielding the hypercube into the subspace it is projected into leads to the set of all hyperplanes tangent to the object color-solid. The dual boundary has the significant advantage over the primal boundary, that individual boundary points can be uniquely parametrized independent of the existence of optimal reflectance functions. It was shown how the dual boundary is related to the metamer mismatch body and how this relation may be used to calculate boundary points of the metamer mismatch body in any chosen direction. The resulting algorithm is abstracted to color mechanisms of arbitrary dimensions, making it applicable to multi-spectral camera-systems.

The proposed algorithm opens the possibility to evaluate datasets robustly in a reproducible way in less time. Additionally, it is able to handle cases where the original theory fails to produce valid results, namely illuminants having zero emission in certain wavelengths.

References

[1] A. D. Logvinenko, B. Funt, and C. Godau, "Metamer Mismatching," *Trans. Img. Proc.*, vol. 23, no. 1, pp. 34–43, Jan. 2014. [Online]. Available: http://dx.doi.org/10.1109/TIP.2013.2283148

[2] G. Wyszecki and W. S. Stiles, *Color Science: Concepts and Methods, Quantitative Data and Formulae, 2nd edition*, 1982.

[3] R. Luther, "Aus dem Gebiet der Farbreizmetrik," *Zeitschrift für technische Physik*, vol. 8, pp. 540–558, 1927.

[4] H. E. Ives, *The transformation of color-mixture equations from one system to another*. J. Franklin Inst., 1915.

[5] P. Centore, "An Open-Source Algorithm for Metamer Mismatch Bodies," *unpublished*, 2017.

[6] P. Urban and R.-R.Grigat, "The Metamer Boundary Descriptor Method for Color Correction," *Journal of Imaging Science and Technology*, vol. 49, no. 4, pp. 418–430, 2005.

[7] B. A. Wandell and J. E. Farrell, "Water into wine: converting scanner rgb to tristimulus xyz," vol. 1909, 1993, pp. 1909 – 1909 – 10.

[8] F. Martinez-Verdu, J. Puyol, and P. Capilla, "Characterization of a digital camera as an absolute tristimulus colorimeter," *Journal of Imaging Science and Technology*, vol. 47, no. 4, pp. 279–295, 2003.

[9] M. R. L. Guowei Hong and P. A. Rhodes, "A study of digital camera colorimetric characterization based on polynomial modeling," *Color Research & Application*, vol. 26, no. 1, pp. 76–84, 2001.

[10] Z. Yan, H. Zhang, B. Wang, S. Paris, and Y. Yu, "Automatic Photo Adjustment Using Deep Neural Networks," *ACM Trans. Graph.*, vol. 35, no. 2, pp. 11:1–11:15, 2016.

[11] G. Finlayson and P. Morovic, "Metamer constrained color correction," *Journal of Imaging Science and Technology*, vol. 44, no. 4, pp. 295–+, 2000.

[12] E. Schrödinger, "Theorie der Pigmente von grösster Leuchtkraft," *Annalen der Physik*, vol. 62, pp. 603–622, 1920.

[13] R. Hartley and A. Zissermann, *Multiple View Geometry*, 2nd ed. Cambridge University Press, ISBN: 0521540518, 2004.